nature nanotechnology

ARTICLES

PUBLISHED ONLINE: 20 OCTOBER 2013 | DOI: 10.1038/NNANO.2013.209

A general strategy for the DNA-mediated self-assembly of functional nanoparticles into heterogeneous systems

Yugang Zhang[1], Fang Lu[1], Kevin G. Yager[1], Daniel van der Lelie[2] and Oleg Gang[1]*

Nanoparticles coated with DNA molecules can be programmed to self-assemble into three-dimensional superlattices. Such superlattices can be made from nanoparticles with different functionalities and could potentially exploit the synergetic properties of the nanoscale components. However, the approach has so far been used primarily with single-component systems. Here, we report a general strategy for the creation of heterogeneous nanoparticle superlattices using DNA and carboxylic-based conjugation. We show that nanoparticles with all major types of functionality—plasmonic (gold), magnetic (Fe_2O_3), catalytic (palladium) and luminescent (CdSe/Te@ZnS and CdSe@ZnS)—can be incorporated into binary systems in a rational manner. We also examine the effect of nanoparticle characteristics (including size, shape, number of DNA per particle and DNA flexibility) on the phase behaviour of the heterosystems, and demonstrate that the assembled materials can have novel optical and field-responsive properties.

Heterogeneous superlattices[1,2] built from functional nanoscale building blocks such as metallic, semiconducting and magnetic nanoparticles are of interest for the creation of novel materials with emergent and collective properties; for example related to coherent vibration[3], enhanced ferro- and ferrimagnetism[4,5], optical response[6–8], high-energy nanocomposites[9] and robust mechanical properties[10]. Self-assembly methods have been successfully applied to create binary[11–13] and ternary[14] superlattices, exploiting entropic effects, electrostatics and van der Waals forces. However, the determinant driving forces for assembly are highly system-specific. Moreover, the majority of approaches lack the flexibility to regulate interparticle distances, which is highly relevant for tuning functional properties, for example, for metal nanoparticle-enhanced photoluminescence[15], super-spin data storage[16] and metamaterials[11,17,18].

DNA-driven nanoparticle assembly is an effective approach for the fabrication of superlattices with tunable interparticle distances[1,2,19,20] and rich phase behaviour[21,22]. The high specificity of DNA recognition permits the programming of nanoparticle interconnections, which allows for assembly processes to be decoupled from the intrinsic properties of the particle core. Experimentally, however, gold nanoparticles have long served as the focal component for DNA-mediated nanoparticle assembly, for which crystallization was realized by tailoring the DNA shell[1,2,23,24] and nanoparticle shape[25] and size[26]. Although there have been several recent efforts to incorporate other components, such as dyes[7], proteins[27] and CdSe/ZnS quantum dots[28,29], into gold-nanoparticle lattices and clusters[15,30], a broadly applicable DNA-based methodology for the rational fabrication of heterosystems and multifunctional materials is required. Recent studies have reported the assembly of multicomponent lattices[12,31–33]. However, from a fundamental perspective, it remains unclear to what degree the principles governing such assemblies are generalizable. For example, heterogeneity in particle core size, shape, and also ligand shells, can tremendously affect packing behaviour.

We have developed a general strategy for DNA-mediated self-assembly of binary heterogeneous systems comprising four representative functional nanoparticles: plasmonic, catalytic, magnetic and luminescent. Accordingly, we selected the following model systems: spherical gold with palladium of three shapes (cube, octahedron and dodecahedron-like), iron oxide (Fe_2O_3, denoted FeO) and quantum dots of different materials (CdSe/CdTe/@ZnS and CdSe/ZnS). By combining these components into heterolattices, we address three major assembly issues: (1) the role of shape heterogeneity on lattice order, (2) the interplay between DNA-programmable and non-specific interactions, and (3) the emergence of compositional disorder in multicomponent lattices. Our studies demonstrate that heterogeneous nanosystems with regulated interparticle separations can be assembled in a 'mix-and-match' manner, which opens remarkable opportunities for material fabrication.

Our methodology for nanoparticle functionalization with DNA comprises three steps: carboxylic group grafting, streptavidin conjugation and biotinylated-DNA attachment (Fig. 1a). We illustrate the versatility of this strategy for both hydrophilic and hydrophobic nanoparticles (see Methods). Using this method, f DNAs were tethered onto each palladium (Fig. 1c, Supplementary Fig. 1), FeO (Fig. 1d, Supplementary Fig. 2) and quantum dot (Fig. 1e, Supplementary Fig. 3) particle ($f = 20 \pm 5$, 4 ± 2 and 30 ± 10, respectively). All these DNA-functionalized nanoparticles were thermally stable at the highest temperatures tested ($\sim$70 °C, Supplementary Fig. 5). We also functionalized citrate-capped gold nanoparticles (Fig. 1f, Supplementary Fig. 4) with thiolated-DNA ($f \approx 50 \pm 10$ for 10 nm gold). Two strategies were then applied for nanoparticle assembly: direct hybridization (DH) or linker-assisted hybridization (LH)[34], as illustrated schematically in Fig. 1b. In a DH system, denoted $A\_B_{XA\_XB}$, the particle surfaces are separated by $N = X_A + X_B + 15$ bases. For LH systems, denoted A_B_{Ln}, $N = X_A + X_B + L_n + 30$ bases (see Supplementary Section 'Materials and methods' for preparation details).

Synchrotron-based small-angle X-ray scattering (SAXS, performed at BNL NSLS X9) was used to probe the *in situ* structure of particles assemblies. The featureless SAXS scattering profiles

[1]Center for Functional Nanomaterials, Brookhaven National Laboratory, Upton, New York 11973, USA, [2]Center for Agricultural and Environmental Biotechnology, Research Triangle Institute International, Research Triangle Park, North Carolina 12194, USA. *e-mail: ogang@bnl.gov

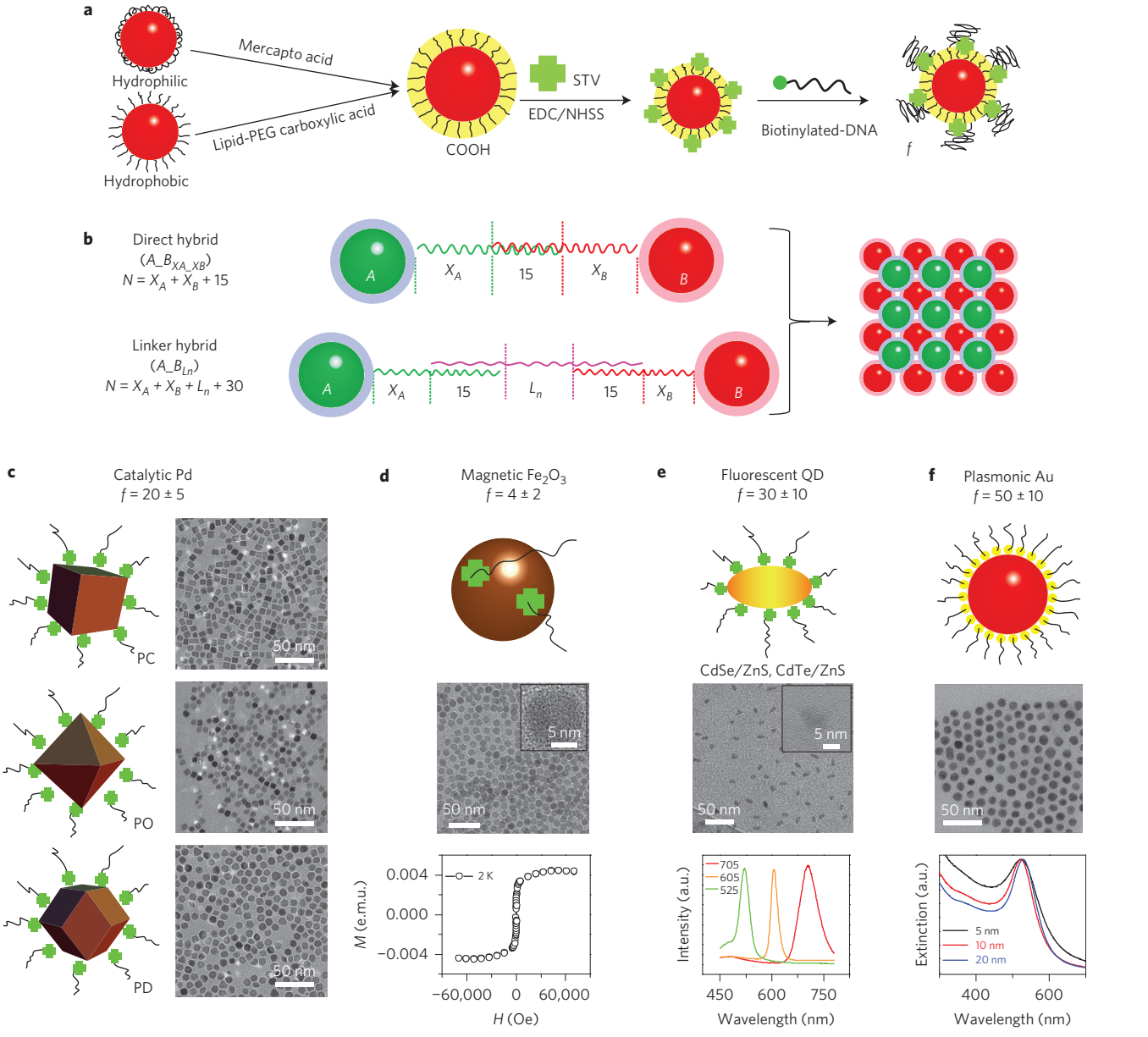

Figure 1 | DNA conjugation and assembly of functional nanoparticles. a, Illustration of the three-step strategy for DNA functionalization of hydrophilic and hydrophobic nanoparticles (*f* denotes the number of grafting DNA on nanoparticles; see Supplementary Section 'Materials and methods'). STV, streptavidin; NHSS, *N*-hydroxysulfosuccinimide; EDC, 1-ethyl-3-(3-dimethylaminopropyl)carbodiimide. **b**, Schematics of two kinds of assembly strategy, direct hybrid (DH) and linker hybrid (LH). **c**, Schematics and SEM images for biotinylated DNA-tethered palladium nanocube (PC), octahedron (PO) and dodecahedron (PD). All three types of palladium nanoparticle were originally coated with PVP. **d**, Schematic, TEM image (inset is HRTEM) and magnetic hysteresis loop for biotinylated DNA-grafted Fe_2O_3 (denoted FeO) nanoparticles originally capped by OA. **e**, Schematic and TEM image (inset is HRTEM) for Q7, and photoluminescence spectra for biotinylated DNA-attached CdSe/ZnS quantum dots (QD525, denoted Q5, and QD605, denoted Q6) and CdTe/ZnS quantum dots (Q705, denoted Q7). All three types of quantum dot were originally coated with TOPO. **f**, Schematic, TEM image (for 10 nm gold nanoparticles) and ultraviolet–visible spectra for thiolated DNA-functionalized gold nanoparticles (5, 10 and 20 nm), originally capped by citrate.

(Supplementary Fig. 6) for control systems, which involve non-complementary surface-tethered DNA, demonstrate that DNA interactions are the driving force for assembly. The multicomponent systems in our studies, catalytic–plasmonic, magnetic–plasmonic and fluorescent–plasmonic, were designed to address the role of shape heterogeneity, non-specific interactions and compositional disorder, respectively.

Systems of catalytic and plasmonic nanoparticles

To investigate the effect of particle shape in binary heterolattices, 10 nm spherical gold nanoparticles were coupled to ~11 nm palladium nanoparticles of different shapes: cubic (PC), octahedral (PO) and dodecahedral (PD). This allowed us to probe a central question for heterogeneous systems: to what degree can differently shaped particles coexist in the superlattice? While mixing particle shapes can often result in phase separation, driven by maximum packing requirements and entropic effects, the situation is quite different for DNA-complementary particles, which benefit energetically from the mixing.

We first explored shape heterogeneity effects in short-DNA systems. The structure factors $S(q)$ for each of PC, PO and PD with gold in DH systems ($N = 33$) are provided in Fig. 2a (top panel). Distinct from hard-core particle packing results[35], all three systems displayed similar structures, albeit with different correlation

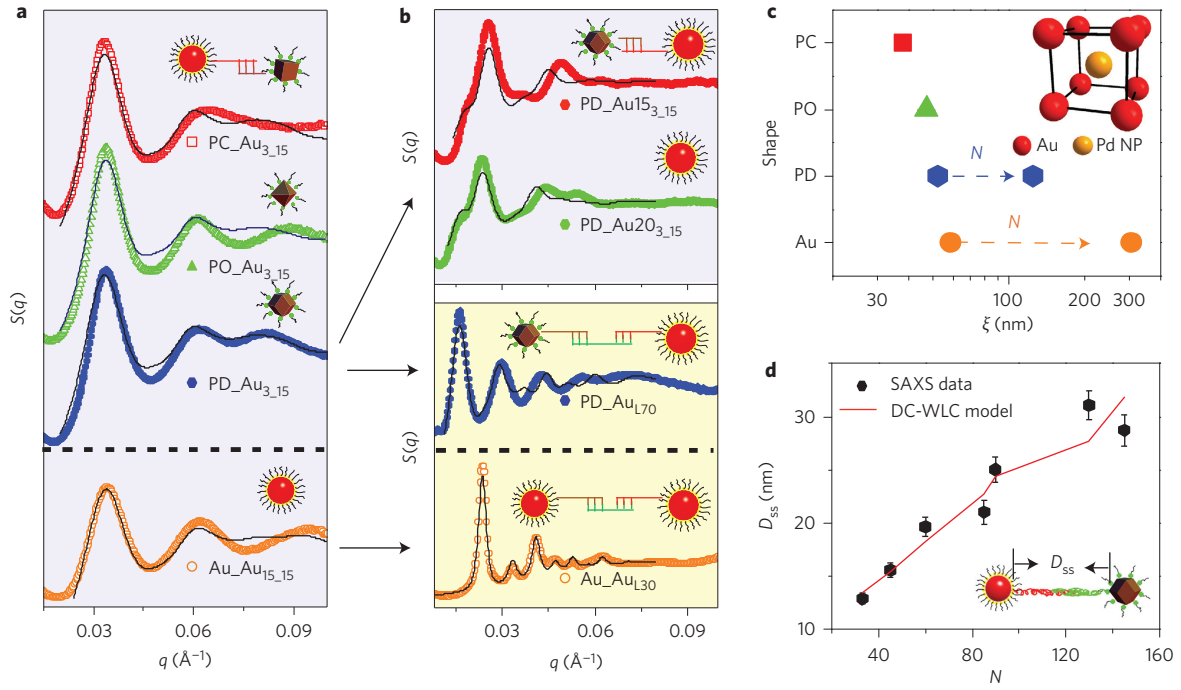

Figure 2 | Systems of palladium and gold nanoparticles. a, Shape-dependent structure factors ($S(q)$) extracted from SAXS patterns of DH systems with short DNA. PC_Au_{3_15}, PO_Au_{3_15}, PD_Au_{3_15} and Au_Au_{15_15} correspond to systems assembled using 10 nm spherical gold nanoparticles with cube- (PC), octahedron- (PO) and dodecahedron- (PD) shaped palladium and spherical gold nanoparticles, respectively. For all $S(q)$ figures in this Article, coloured symbols represent SAXS data and black solid lines correspond to fits (vertically offset for clarity). **b**, Top: gold nanoparticle size-dependent $S(q)$ evolution of PD–Au DH systems, including PD hybridized with 15 nm gold for PD_$Au15_{3_15}$ and 20 nm gold for PD_$Au20_{3_15}$. Different ordering states are obtained for PD–Au (middle) and Au–Au (bottom) by using longer DNA. **c**, Effects of nanoparticle shape on correlation length ξ of binary lattices. Square (red), triangle (green), hexagon (blue) and circle (orange) symbols correspond to systems built from gold nanoparticles with PC, PO, PD and spherical gold nanoparticles, respectively. Spherical nanoparticles favour better structures. Inset: schematic for the formed binary CsCl-type lattice. **d**, Nearest-neighbour particle surface-to-surface distance D_{ss}, as illustrated in the inset for PD–10 nm gold systems (error bars correspond to one standard deviation for repeated experiments). The line represents the values calculated by a combination of the Daoud–Cotton (DC) blob model and a worm-like chain (WLC) model.

lengths ξ. As shown in Fig. 2c, ξ increases slightly when the particle shape changes from PC to PO and PD, indicating that a more spherical shape promotes longer-range order. The trend was further verified by substitution of palladium with spherical gold nanoparticles (Au_Au_{15_15}), which resulted in a further increase in ξ to ~60 nm (Fig. 2a, bottom panel). In addition to shape effects, the disruption of long-range order could also be related to the surface distribution of tethered ligands[36] on the particle facets.

Our study of both DH and LH PD–Au systems (Supplementary Fig. 7a) indicates that the softer single-stranded DNA shells reduce shape heterogeneity. Indeed, we observed a monotonic increase of $\xi(N)$ to ~90 nm in PD–Au DH systems and 130 nm in LH systems (Supplementary Fig. 8) with an increase in DNA length. However, systems containing only spherical particles exhibit even better order, for example $\xi \approx 310$ nm (Au_Au_{L30}, Fig. 2b, bottom panel). This difference in ξ between systems with heterogeneous and homogeneous shapes might be related to an incompatibility between particle geometry and lattice symmetry, or to a more complex kinetic pathway to crystallization[35]. Previous studies have shown that nanoparticle shells can induce a phase transformation due to edge rounding[37] and can lead to ribbon morphologies[38] and tighter separations[39] due to the collective chain effects. This work demonstrates that soft shells can promote lattice order by masking the shape of the cores. Presently, we focus on systems with similar particle sizes (~10 nm). An interesting topic for future investigations is the effect of the particle size ratio on lattice structure for binary systems of heterogeneously shaped particles.

Our detailed structure analysis (Supplementary Section 'Modelling of SAXS profiles') indicates a weakly ordered CsCl lattice for all the Pd–Au systems (Fig. 2a,b). This assignment was further confirmed for PD systems with 15 and 20 nm gold particles. In contrast to the 10 nm gold case, a (100) peak (Fig. 2b, top), located at $\sim 1/\sqrt{2}$ of the (110) peak, gradually emerges with an increase of size from 15 to 20 nm. This $S(q)$ trend is consistent with a CsCl lattice containing nanoparticles with different electron densities[28], as discussed in detail below for quantum dot (QD)–Au systems. No particle segregation was observed for the assembled systems, and scanning electron microscopy (SEM) imaging (Supplementary Fig. 7b) and energy dispersive X-ray spectroscopy (EDS) mapping (Supplementary Fig. 7c) revealed a uniform distribution of palladium and gold elements in dried samples, with a ratio of ~1:1.

The lattice constant can be effectively controlled by the DNA length N, and the observed dependence of $D_{ss}(N)$, the nearest-neighbour particle surface-to-surface distance, is well-described by the Daoud–Cotton (DC) model (Supplementary Section 'DNA modelling' and Supplementary Table 2), neglecting particle geometry (Fig. 2d). This ability to regulate the distances is advantageous for coupling of optical excitations with catalytic activity, and for regulated mass transport.

Systems of magnetic and plasmonic nanoparticles

Superlattices constructed from FeO and gold nanoparticles of similar sizes (~10 nm) can exhibit both magnetic and plasmonic properties. We use this system to study the role of competition between specific DNA-encoded interactions and non-specific interactions, such as magnetic and van der Waals forces.

We first investigated the behaviour of a pure FeO nanoparticles system. Owing to the small number of DNA in their shells and

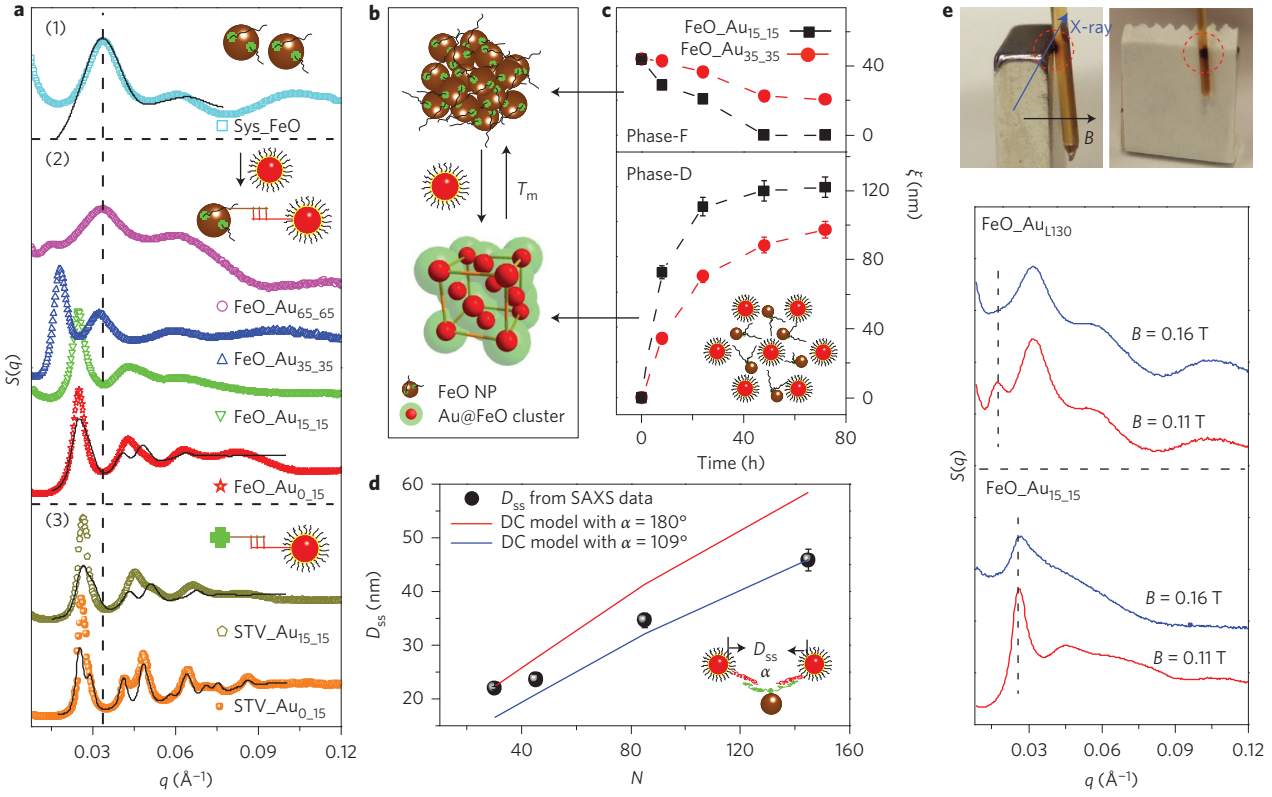

Figure 3 | Systems of FeO and gold nanoparticles. a, (1) $S(q)$ for non-specific interaction-induced FeO aggregates. This system and its structure are denoted by Sys_FeO and Phase-F, respectively. (2) DNA base number (N)-dependent evolution of $S(q)$ from the single-component Phase-F to a DNA-directed Au–FeO binary superlattice (with structure denoted as Phase-D) upon introducing complementary gold nanoparticles. (3) $S(q)$ for a DH system assembled by streptavidin and gold nanoparticles with longer and shorter DNA. **b**, Three-dimensional schematic illustration of structural switching between Phase-F (fcc arrangement of FeO nanoparticles) and Phase-D (fcc Au–FeO lattice) by introducing gold nanoparticles or elevating the temperature. **c**, Assembly kinetics for Phase-F and Phase-D from $FeO\_Au_{15\_15}$ and $FeO\_Au_{35\_35}$. Inset: two-dimensional schematic for Phase-D. **d**, Closed circles indicate D_{ss} for FeO–Au DH systems, provided by SAXS data. Lines present values from DC-WLC modelling with $\alpha = 180^\circ$ and 109°. Inset: definition of D_{ss} and α in the Au–FeO superlattice. **e**, Top: experimental configuration for SAXS measurement in a magnetic field (0.11 T or 0.16 T). Bottom: $S(q)$ magnetic response for $FeO\_Au_{15\_15}$ and FeO_Au_{L130}.

their inherent magnetic properties, aggregates readily form in FeO solutions. A representative $S(q)$ (Fig. 3a,1) can be fitted with a weakly ordered face-centred cubic (fcc) lattice, denoted Phase-F. This phase is thermally stable to the highest tested temperature of ~70 °C. Interestingly, the introduction of gold nanoparticles into FeO aggregate solutions converts the Phase-F into a binary FeO–Au phase, denoted Phase-D. Moreover, the kinetics of the conversion process, and the final phase, are controlled by DNA length. Figure 3a,2 shows an $S(q)$ series for different DH systems, where N decreases from 145 to 30. Shorter DNA motifs favour a larger fraction of Phase-D (N = 45 ($FeO\_Au_{15\_15}$) and 30 ($FeO\_Au_{0\_15}$)), while longer DNA connectors (N = 145 ($FeO\_Au_{65\_65}$) and 70 ($FeO\_Au_{35\_35}$)) produce a mixture of phases. Similar behaviour was observed for LH systems (Supplementary Fig. 12). The new phase is driven by DNA hybridization between nanoparticles, as confirmed by thermal-reversible dissociation–association behaviour (Fig. 3b, Supplementary Figs 9a,10,11) and the restoration of Phase-F above DNA melting, T_m (~55 °C).

The conversion into Phase-D at the expense of the initial Phase-F is further revealed by kinetic studies. By monitoring $S(q)$ upon introducing complementary gold (N = 45 and 85) into Phase-F (Supplementary Fig. 13,14), we extracted the time evolution of ξ for both phases (Fig. 3c). Systems with shorter DNA display faster formation of Phase-D and a complete elimination of Phase-F at ~40 h, whereas for systems with longer DNA this requires weeks. The slower kinetics and smaller ξ for longer-DNA systems can be attributed to a larger penetration barrier into Phase-F due to a higher entropic penalty.

Structural analysis suggests that the Phase-D is formed by gold particles in an fcc lattice in which numerous FeO particles surround the gold particles (a fit is shown as a black solid line in Fig. 3a,2). Consistent with this scheme, the EDS results (Supplementary Fig. 7b,c) for Phase-D indicate a more than tenfold higher concentration of FeO than gold in the lattice. To reveal the possible placement of FeO, we examined a DNA-linked Au–streptavidin system. Such comparison is meaningful due to the small number of DNA linkages with gold for both streptavidin and FeO nanoparticles. Figure 3a,3 shows an $S(q)$ of two Au–streptavidin DH systems with different N, where the number ratio of streptavidin to gold is ~20. A remarkable similarity is observed between FeO–Au and corresponding streptavidin–Au systems: shorter DNAs result in higher structural order. The Au–streptavidin scattering is well-described by a gold fcc lattice. Considering the large ratio of FeO (or streptavidin) to gold, the fcc-type frame of gold nanoparticles can be stabilized by the numerous FeO (or streptavidin) surrounding each gold particle, which also connect them (Fig. 3b). A possible arrangement of FeO can be obtained from the $D_{ss}(N)$ dependence (Fig. 3d). Schematically, FeO links two gold nanoparticles with an angle α formed between two adjacent Au–FeO connections. The D_{ss} data are well-described by this structural model, with α varying from 180° (red line, Fig. 3d) to 109° (blue line), suggesting that FeO can act as linear and tetrahedral bridges between gold nanoparticles.

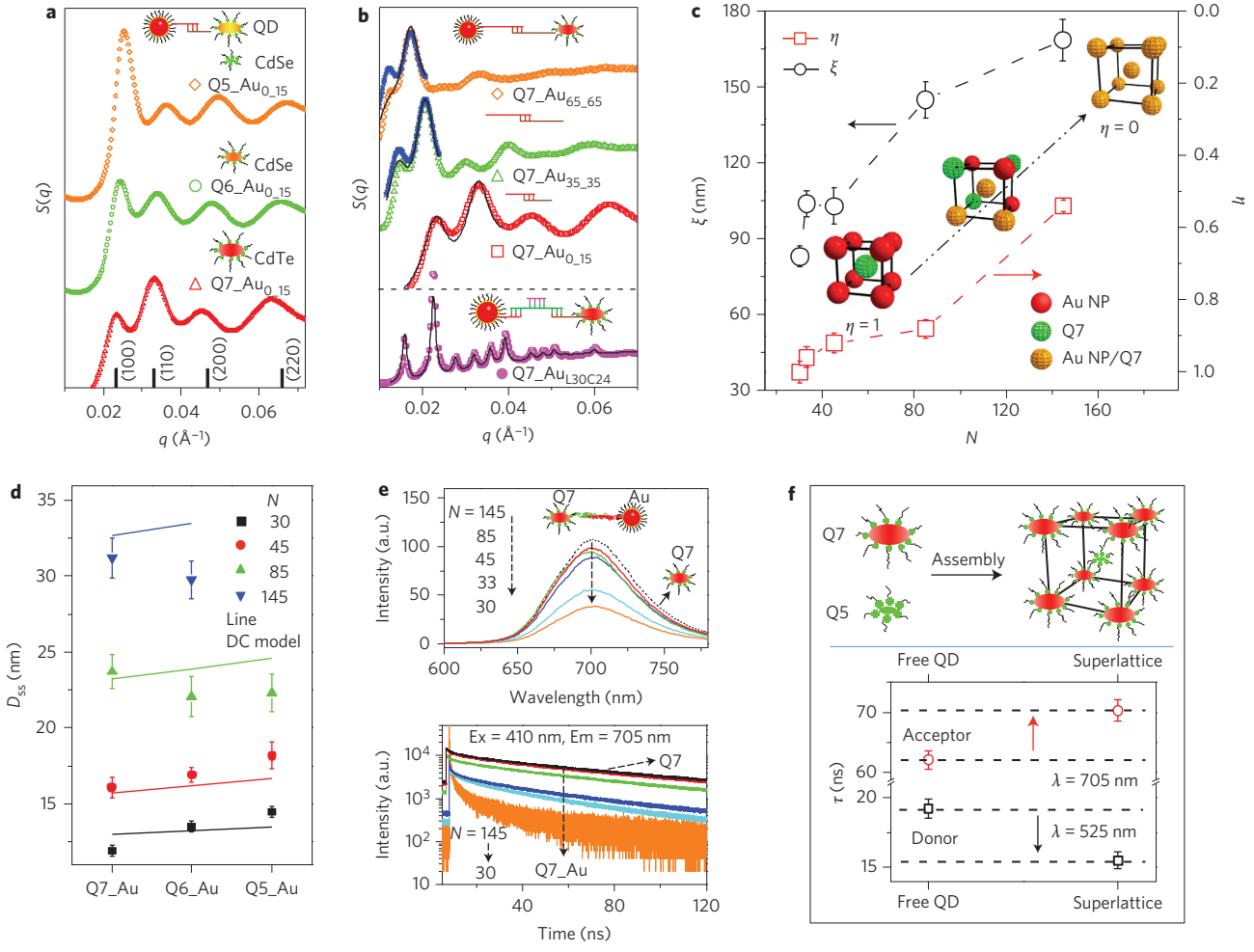

Figure 4 | Systems of quantum dots and gold nanoparticles. a, Component-dependent $S(q)$ evolution of DH systems. Q7_Au_{0_15}, Q6_Au_{0_15} and Q5_Au_{0_15} correspond to gold nanoparticles hybridized with Q7, Q6 and Q5, respectively. **b**, Top: DNA-spacer length-dependent $S(q)$ of Q7–Au systems (Q7_Au_{0_15}, Q7_Au_{35_35} and Q7_Au_{65_65}). Bottom: $S(q)$ of a well-ordered Q7–Au system $Q7A_{L30C24}$, which has both flexible and rigid DNA regions. Black solid lines and blue markers correspond to fits with and without consideration of compositional order. **c**, Variation of compositional order parameter η and correlation length ξ with DNA base number N for DH Q7–Au systems. Inset: compositional OTD transition with η from 1 to 0 in a CsCl lattice formed in the binary gold and quantum dot systems. NP, nanoparticle. **d**, D_{ss} for QD–Au DH systems. Open circles are SAXS data, and the line is calculated using the DC model. **e**, Steady-state and time-resolved photoluminescence spectra collected from Q7_Au DH systems, including a change in N from 145 to 85, 45, 33 and 30 and a free dispersed biotinylated-DNA-capped Q7 solution. The quenching efficiency, $E = 1 - (\tau_s/\tau_f) \approx 0.74$ for $N = 30$, where τ_s and τ_f are the lifetimes of free and in-superlattice quantum dots. **f**, Lifetime τ for donor (Q5) and acceptor (Q7) in the free-dispersed states and superlattice Q7_$Q5_{3_3}$. The sketch shows a CsCl lattice formed by Q7 and Q5 directed by DNA.

We also probed the magnetic response of such systems (Phase-D (FeO_Au_{15_15}) and mixed Phase-F and Phase-D (FeO_Au_{L130})). For Phase-D, an increase in magnetic field B results in a broadening of the first $S(q)$ peak and the disappearance of higher-order peaks—hallmarks of disorder. For the mixed phase, a more profound response is observed for Phase-D, with the phase disappearing at 0.16 T. Interestingly, both systems demonstrate fully reversible phase restoration when the field is removed. The softer interparticle potentials arising from a smaller number of longer DNA linkages might be responsible for the larger responsiveness of FeO_Au_{L130}. Thus, while the non-specific interactions can interfere with DNA-driven assembly, the specific DNA-encoded interactions can be optimized to overcome this limitation. Moreover, there are interesting opportunities for designing materials where phases are both temperature- and field-responsive.

Systems of luminescent and plasmonic nanoparticles

Nanomaterials comprising quantum dots and plasmonic nanoparticles are not only attractive for novel optical responses, but are also suitable for addressing fundamental structural issues such as compositional disorder in binary superlattices[28]. We demonstrate here QD–Au lattice assemblies using three types of quantum dot: Q5 and Q6 from CdSe@ZnS and Q7 from CdSe/Te@ZnS, with corresponding sizes of 2.5 ± 0.6, 4.5 ± 0.8 and 6.5 ± 0.9 nm and emissions at 525, 605 and 705 nm. The functionalization of quantum dots with DNA using streptavidin results in ~30 DNA chains per quantum dot, which is higher than an optimized carboxylic–amine conjugation[40]. Systems (Q7_Au_{0_15}, Q6_Au_{0_15} and Q5_Au_{0_15}) built with short ($N = 30$) DNA show $S(q)$ with similar ratios between peak positions, which can be indexed as CsCl lattices (Fig. 4a). Substitution of quantum dots from Q5 to Q6 or to Q7 has a profound effect on the peak intensity ratio, $S(110)/S(100)$, due to electron density differences.

By changing the DNA length N, we fabricated a family of lattices for all types of quantum dots (Fig. 4b, Supplementary Figs 15–18) with D_{ss} (Fig. 4d) suitable for plasmonic effects (~12 to 31 nm). Interestingly, N affects ξ, which monotonically increases with N (Fig. 4c). More strikingly, the $S(110)/S(100)$ ratio also gradually

grows with N for Q7–Au (Fig. 4b, Supplementary Figs 15,16). Analogous behaviour is observed for other quantum-dot systems (Supplementary Figs 17,18). The change of $S(110)/S(100)$ can be attributed to a compositional order-to-disorder (OTD) transition, which has been extensively studied in atomic systems and has been predicted in DNA-assembled systems[41]. We parameterize the OTD with a compositional order parameter, $\eta = (r_A - F_A)/(1 - F_A)$, where r_A is fraction of A sites occupied by A particles, and F_A is the fraction of A particles in the lattice. Thus, $\eta = 1$ corresponds to perfect compositional order and $\eta = 0$ to disordered lattices. By fitting the first two $S(q)$ peaks (Supplementary Section 'Modelling of SAXS profiles' and Supplementary Fig. 16) we obtained $\eta(N)$ for Q7–Au systems (Fig. 4c). We reveal the development of compositional disorder: η decreases from ~0.98 to ~0.54 with a corresponding increase in N from 30 to 145. Remarkably, larger N favours a better lattice order (larger ξ), even while it induces more compositional disorder; that is, quantum dot and gold sites are exchanged in the CsCl lattice (Fig. 4c). Both trends can be related to softness of the interparticle repulsive potential[1,21], although quantitative understanding of this transition will require detailed theoretical studies. The crucial role of particle softness was verified in our experiments using LH with rigid DNA, Q7_Au_{L30C24}, for which a high degree of order ($\xi > 700$ nm) and no compositional disorder ($\eta \approx 1$) are observed (Fig. 4b, bottom). We note that compositional disorder might play an important role in the optical properties of superlattices due to the high sensitivity of emitters to the number of plasmonic nanoparticles in close proximity[7].

To demonstrate the utility of the approach for material fabrication, we probed the photoluminescence of QD–Au systems (Q7_Au DH with N from 145 to 30). Steady-state and time-resolved photoluminescence spectra (Fig. 4e) show progressive photoluminescence quenching of quantum dots with a decrease in N, which is accompanied by the fluorescence lifetime τ decreasing from 62.1 ns for free quantum dots to as little as 16.6 ns for $N = 30$. In another example, we explore binary QD–QD lattices in which donor (Q5) and acceptor (Q7) nanoparticles are separated by $D_{ss} \approx 15$ nm (Fig. 4f, Supplementary Fig. 22). An energy transfer was observed with ~20% decrease in donor lifetime and ~12% increase in acceptor lifetime. Thus, the presented approaches open unique opportunities for exploration and tailoring of optical properties of three-dimensional materials.

Binary systems without gold

The approach used above to generate gold nanoparticle-based heterogeneous lattices is equally suited to the formation of binary systems with arbitrary combinations of nanoparticles. We found that the number of grafted DNA per nanoparticle, f, plays a crucial role in deciding the assembly behaviour. For example, quantum dots of three types ($f = 30 \pm 10$) and palladium of three shapes ($f = 20 \pm 5$) form superlattices, but FeO systems ($f = 4 \pm 2$) typically only form sub-100 nm clusters. The thermally reversible superlattices of representative systems (QD–QD, Pd–Pd, Pd–QD, Supplementary Figs 19–21) show CsCl organizations with quite different degrees of structural order, consistent with recent results[24,26] for particles of similar sizes.

In Fig. 5a we summarize the phase diagram, shown in coordinates of nanoparticle-grafted DNA numbers f_A and f_B, for all the studied binary A–B systems with nominal nanoparticle sizes of ~10 nm. Several important conclusions can be drawn for materials designed based on DNA assembly. (1) f_A and f_B control assembly morphology, which can vary from finite-sized clusters ($f_A + f_B < 30$) to weakly ordered ($30 < f_A + f_B < 70$–80) and well-ordered lattices ($f_A + f_B > 70$–80). (2) For systems involving nanoparticles with the non-specific interactions (for example, FeO), a shorter DNA length is essential to the efficient triggering of DNA-driven assembly. (3) For heterogeneous assembly, quasi-spherical nanoparticles (for example, dodecahedral) are preferable for improved ordering; however, the particle shape can be masked to some extent by increasing the thickness of the single-stranded DNA (ssDNA) shell. (4) For systems with distinctively different f_A and f_B (for example, gold and quantum dots), shorter ssDNA motifs promote compositional order while longer ones result in better long-range lattice ordering. However, for low f, compositional disorder is dominant event for short motifs (for example, QD–Pd, Supplementary Fig. 21).

From a material perspective, Fig. 5 demonstrates that multifunctional binary systems can be formed from functionally diverse components (for example, plasmonic, fluorescent, catalytic and magnetic). We emphasize that the design rules outlined above are not necessarily restrictive, because a high degree of lattice order is

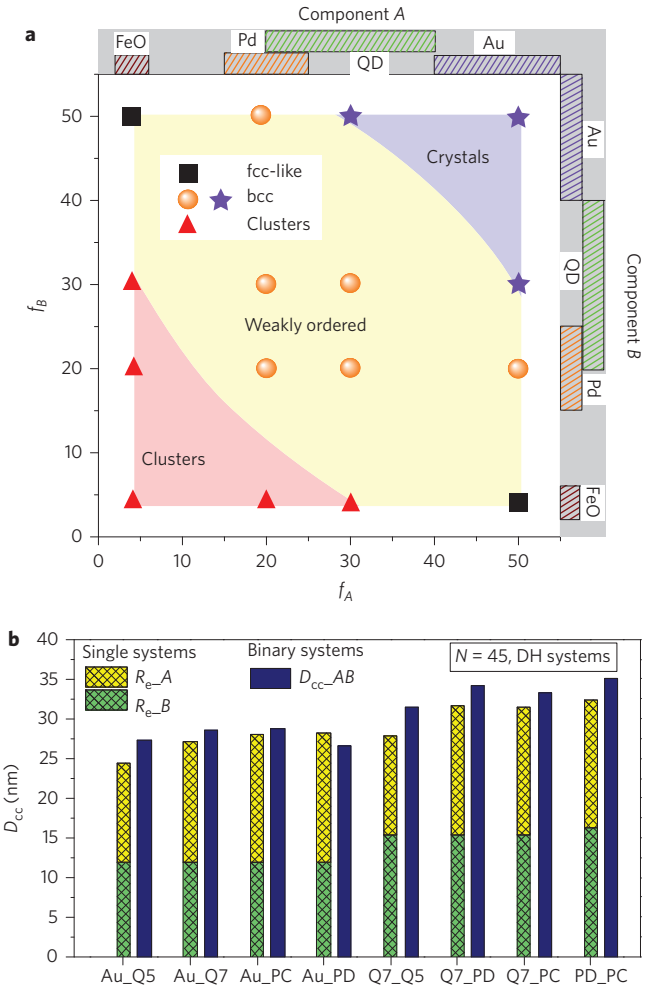

Figure 5 | Phase diagram and interparticle distance for heterogeneous systems. a, Phase diagram for our heterogeneous binary systems of functional (magnetic FeO, catalytic palladium, fluorescent quantum dot and plasmonic gold) components. Leading parameters of the phase diagram for similarly sized particles are the numbers of DNA per particle, f_A and f_B, as discussed in the main text. fcc, face-centred cubic; bcc, body-centred cubic. **b**, 'Mix-and-match' assembly for the predictable interparticle centre-to-centre distances (D_{cc}) for heterosystems. The example of a DH system with $N = 45$ is shown. The effective radii R_e_A and R_e_B of five components (gold, Q7, Q5, PD and PC nanoparticles) were obtained from SAXS data for single-component systems. Dark blue bars correspond to the SAXS-measured D_{cc} for binary superlattices.

not required for many material applications. For example, plasmonic effects are determined by local nanoparticle environment[7], metamaterial properties depend on average nanoparticle density[42], and high-energy nanocomposites require homogeneous nanoparticle mixing[9]. Thus, all types of morphologies from clusters to weakly- and well-ordered lattices can find their niche. At the same time, the control of interparticle distance is important for system functionality. To this end, we found that interparticle distances in binary systems D_{cc}_AB (Fig. 5b) are well estimated by accounting for the nanoparticle effective radius $R_e\_A = D_{cc}\_A/2$, where D_{cc}_A is for a single-component system and $D_{cc}\_AB = D_{cc}\_A + D_{cc}\_B$. The observed D_{cc}_AB also agrees with the discussed DC models (Supplementary Section 'DNA modelling' and Supplementary Table 2). Such predictable control of interparticle separation combined with a 'mix-and-match' material assembly methodology promises to rationalize the fabrication of two-component nanoparticle systems using DNA programmability.

In summary, we have presented a general approach for DNA functionalization and assembly of functional nanoparticles, as well as demonstrating the leading factors influencing the phase behaviour of created systems. We have produced examples of multifunctional and field-responsive superlattices that include representative classes of magnetic, catalytic, fluorescent and plasmonic nanocomponents.

Methods

Synthesis, DNA conjugation and assembly of functional nanoparticles. The hydrophilic poly-vinyl-pyrrolidone (PVP)-capped palladium and hydrophobic oleic acid (OA)-capped iron oxide were synthesized according to reported procedures with modifications (Supplementary Section 'Materials and methods'). The initial particles used in this study were PVP-capped catalytic palladium[43] (Fig. 1c, Supplementary Fig. 1), OA-capped magnetic FeO (Fig. 1d, Supplementary Fig. 2) and trioctylphosphine oxide (TOPO)-capped fluorescent quantum dots (provided by Invitrogen; Fig. 1e, Supplementary Fig. 3).

The nomenclature and sequences of DNA used in this work are provided in Supplementary Table 1. DNA strands were purchased from Integrated DNA Technologies. The three-step DNA functionalization strategy, namely carboxylic group grafting, streptavidin conjugation and biotinylated-DNA attachment, and the assembly and crystallization of nanoparticles are fully described in Supplementary Section 'Materials and methods'. Our control experiments show that streptavidin and DNA are not released from the particle surface (Supplementary Fig. 5) on heating to 70 °C, which confirms the thermal stability of the DNA conjugations.

Characterization of nanoparticles and assemblies. The morphology and microstructure of nanoparticles were characterized by electron microscopy. The grafting DNA number on the nanoparticle surfaces was determined based on the reported fluorescence-based method (Supplementary Section 'Quantification of the grafting DNA number'). Synchrotron-based SAXS (NSLS X9) was used to probe the *in situ* structure of particle assemblies.

Modelling of DNA structure and SAXS profiles. We used a Daoud-Cotton (DC) blob model and a worm-like chain (WLC) model to calculate the tethered DNA thickness and linker length, respectively. To simulate powder SAXS profiles, we developed a scattering formalism, which accounted for particle size, shape, and its material, particle polydispersity, lattice disorder and average grain size within the unit cell. All DNA and SAXS modelling details are provided in the Supplementary Information.

Received 20 November 2012; accepted 16 September 2013; published online 20 October 2013; corrected online 23 October 2013

References

1. Nykypanchuk, D., Maye, M. M., van der Lelie, D. & Gang, O. DNA-guided crystallization of colloidal nanoparticles. *Nature* **451,** 549–552 (2008).
2. Park, S. Y. *et al.* DNA-programmable nanoparticle crystallization. *Nature* **451,** 553–556 (2008).
3. Courty, A., Mermet, A., Albouy, P. A., Duval, E. & Pileni, M. P. Vibrational coherence of self-organized silver nanocrystals in f.c.c. supra-crystals. *Nature Mater.* **4,** 395–398 (2005).
4. Sun, S. H., Murray, C. B., Weller, D., Folks, L. & Moser, A. Monodisperse FePt nanoparticles and ferromagnetic FePt nanocrystal superlattices. *Science* **287,** 1989–1992 (2000).
5. Cheon, J. *et al.* Magnetic superlattices and their nanoscale phase transition effects. *Proc. Natl Acad. Sci. USA* **103,** 3023–3027 (2006).
6. Maye, M. M., Nykypanchuk, D., Cuisinier, M., van der Lelie, D. & Gang, O. Stepwise surface encoding for high-throughput assembly of nanoclusters. *Nature Mater.* **8,** 388–391 (2009).
7. Xiong, H. M., Sfeir, M. Y. & Gang, O. Assembly, structure and optical response of three-dimensional dynamically tunable multicomponent superlattices. *Nano Lett.* **10,** 4456–4462 (2010).
8. Kuzyk, A. *et al.* DNA-based self-assembly of chiral plasmonic nanostructures with tailored optical response. *Nature* **483,** 311–314 (2012).
9. Severac, F., Alphonse, P., Esteve, A., Bancaud, A. & Rossi, C. High-energy Al/CuO nanocomposites obtained by DNA-directed assembly. *Adv. Funct. Mater.* **22,** 323–329 (2012).
10. Podsiadlo, P. *et al.* High-pressure structural stability and elasticity of supercrystals self-assembled from nanocrystals. *Nano Lett.* **11,** 579–588 (2011).
11. Redl, F. X., Cho, K. S., Murray, C. B. & O'Brien, S. Three-dimensional binary superlattices of magnetic nanocrystals and semiconductor quantum dots. *Nature* **423,** 968–971 (2003).
12. Shevchenko, E. V., Talapin, D. V., Kotov, N. A., O'Brien, S. & Murray, C. B. Structural diversity in binary nanoparticle superlattices. *Nature* **439,** 55–59 (2006).
13. Kalsin, A. M. *et al.* Electrostatic self-assembly of binary nanoparticle crystals with a diamond-like lattice. *Science* **312,** 420–424 (2006).
14. Evers, W. H., Friedrich, H., Filion, L., Dijkstra, M. & Vanmaekelbergh, D. Observation of a ternary nanocrystal superlattice and its structural characterization by electron tomography. *Angew. Chem. Int. Ed.* **48,** 9655–9657 (2009).
15. Maye, M. M., Gang, O. & Cotlet, M. Photoluminescence enhancement in CdSe/ZnS–DNA linked-Au nanoparticle heterodimers probed by single molecule spectroscopy. *Chem. Commun.* **46,** 6111–6113 (2010).
16. Hiroi, K., Komatsu, K. & Sato, T. Superspin glass originating from dipolar interaction with controlled interparticle distance among γ-Fe_2O_3 nanoparticles with silica shells. *Phys. Rev. B* **83,** 224423 (2011).
17. Vermolen, E. C. M. *et al.* Fabrication of large binary colloidal crystals with a NaCl structure. *Proc. Natl Acad. Sci. USA* **106,** 16063–16067 (2009).
18. Gardner, D. F., Evans, J. S. & Smalyukh, I. I. Towards reconfigurable optical metamaterials: colloidal nanoparticle self-assembly and self-alignment in liquid crystals. *Mol. Cryst. Liq. Cryst.* **545,** 1227–1245 (2011).
19. Alivisatos, A. P. *et al.* Organization of 'nanocrystal molecules' using DNA. *Nature* **382,** 609–611 (1996).
20. Mirkin, C. A., Letsinger, R. L., Mucic, R. C. & Storhoff, J. J. A DNA-based method for rationally assembling nanoparticles into macroscopic materials. *Nature* **382,** 607–609 (1996).
21. Tkachenko, A. V. Morphological diversity of DNA-colloidal self-assembly. *Phys. Rev. Lett.* **89,** 148303 (2002).
22. Dai, W., Hsu, C. W., Sciortino, F. & Starr, F. W. Valency dependence of polymorphism and polyamorphism in DNA-functionalized nanoparticles. *Langmuir* **26,** 3601–3608 (2010).
23. Macfarlane, R. J. *et al.* Establishing the design rules for DNA-mediated colloidal crystallization. *Angew. Chem. Int. Ed.* **49,** 4589–4592 (2010).
24. Xiong, H. M., van der Lelie, D. & Gang, O. Phase behavior of nanoparticles assembled by DNA linkers. *Phys. Rev. Lett.* **102,** 015504 (2009).
25. Jones, M. R. *et al.* DNA–nanoparticle superlattices formed from anisotropic building blocks. *Nature Mater.* **9,** 913–917 (2010).
26. Macfarlane, R. J. *et al.* Nanoparticle superlattice engineering with DNA. *Science* **334,** 204–208 (2011).
27. Cigler, P., Lytton-Jean, A. K. R., Anderson, D. G., Finn, M. G. & Park, S. Y. DNA-controlled assembly of a NaTl lattice structure from gold nanoparticles and protein nanoparticles. *Nature Mater.* **9,** 918–922 (2010).
28. Sun, D. Z. & Gang, O. Binary heterogeneous superlattices assembled from quantum dots and gold nanoparticles with DNA. *J. Am. Chem. Soc.* **133,** 5252–5254 (2011).
29. Tikhomirov, G. *et al.* DNA-based programming of quantum dot valency, self-assembly and luminescence. *Nature Nanotech.* **6,** 485–490 (2011).
30. Sun, D. Z. *et al.* Heterogeneous nanoclusters assembled by PNA-templated double-stranded DNA. *Nanoscale* **4,** 6722–6725 (2012).
31. Ye, X. C., Chen, J. & Murray, C. B. Polymorphism in self-assembled AB(6) binary nanocrystal superlattices. *J. Am. Chem. Soc.* **133,** 2613–2620 (2011).
32. Kang, Y. J. *et al.* Design of Pt–Pd binary superlattices exploiting shape effects and synergistic effects for oxygen reduction reactions. *J. Am. Chem. Soc.* **135,** 42–45 (2013).
33. Zhang, C. *et al.* A general approach to DNA-programmable atom equivalents. *Nature Mater.* **12,** 741–746 (2013).
34. Xiong, H. M., van der Lelie, D. & Gang, O. DNA linker-mediated crystallization of nanocolloids. *J. Am. Chem. Soc.* **130,** 2442–2443 (2008).
35. Damasceno, P. F., Engel, M. & Glotzer, S. C. Predictive self-assembly of polyhedra into complex structures. *Science* **337,** 453–457 (2012).
36. Ye, X. C. *et al.* Competition of shape and interaction patchiness for self-assembling nanoplates. *Nature Chem.* **5,** 466–473 (2013).

37. Zhang, Y. G., Lu, F., van der Lelie, D. & Gang, O. Continuous phase transformation in nanocube assemblies. *Phys. Rev. Lett.* **107,** 135701 (2011).
38. Vial, S., Nykypanchuk, D., Yager, K. G., Tkachenko, A. V. & Gang, O. Linear mesostructures in DNA–nanorod self-assembly. *ACS Nano* **7,** 5437–5445 (2013).
39. Chi, C., Vargas-Lara, F., Tkachenko, A. V., Starr, F. W. & Gang, O. Internal structure of nanoparticle dimers linked by DNA. *ACS Nano* **6,** 6793–6802 (2012).
40. Sun, D. Z. & Gang, O. DNA-functionalized quantum dots: fabrication, structural, and physicochemical properties. *Langmuir* **29,** 7038–7046 (2013).
41. Knorowski, C., Burleigh, S. & Travesset, A. Dynamics and statics of DNA-programmable nanoparticle self-assembly and crystallization. *Phys. Rev. Lett.* **106,** 215501 (2011).
42. Krishnamoorthy, H. N. S., Jacob, Z., Narimanov, E., Kretzschmar, I. & Menon, V. M. Topological transitions in metamaterials. *Science* **336,** 205–209 (2012).
43. Wilson, O. M., Knecht, M. R., Garcia-Martinez, J. C. & Crooks, R. M. Effect of Pd nanoparticle size on the catalytic hydrogenation of allyl alcohol. *J. Am. Chem. Soc.* **128,** 4510–4511 (2006).

Acknowledgements

Research carried out at the Center for Functional Nanomaterials and National Synchrotron Light Source (Brookhaven National Laboratory) was supported by the US Department of Energy, Office of Basic Energy Sciences (contract no. DE-AC02-98CH10886).

Author contributions

Y.G.Z., F.L., D.v.d.L. and O.G. initiated the concept. Y.G.Z. and O.G. designed the experiments. Y.G.Z. performed the experiments and analysed the data, F.L. contributed to particle functionalization and measurements. Y.G.Z. and O.G. wrote the paper. K.G.Y. contributed to the SAXS modelling and analysis. O.G. supervised the project. All authors discussed the results and commented on the manuscript.

Additional information

Supplementary information is available in the online version of the paper. Reprints and permissions information is available online at www.nature.com/reprints. Correspondence and requests for materials should be addressed to O.G.

Competing financial interests

The authors declare no competing financial interests.